Received: 12 September 2019 | Revised: 10 March 2020 | Accepted: 31 March 2020

DOI: 10.1002/dneu.22742

RESEARCH ARTICLE

WILEY

Resting-state networks of the neonate brain identified using independent component analysis

Olli Rajasilta[1] | **Jetro J. Tuulari**[1,2,3,4] | **Malin Björnsdotter**[5,6] | **Noora M. Scheinin**[1,2] | **Satu J. Lehtola**[1] | **Jani Saunavaara**[7] | **Suvi Häkkinen**[1] | **Harri Merisaari**[7] | **Riitta Parkkola**[8] | **Tuire Lähdesmäki**[9] | **Linnea Karlsson**[1,10] | **Hasse Karlsson**[1,2]

[1]FinnBrain Birth Cohort Study, Turku Brain and Mind Center, Institute of Clinical Medicine, University of Turku, Turku, Finland

[2]Department of Psychiatry, University of Turku and Turku University Hospital, Turku, Finland

[3]Department of Psychiatry, University of Oxford, Oxford, UK

[4]Turku Collegium for Science and Medicine, University of Turku, Turku, Finland

[5]The Sahlgrenska University Hospital, Gothenburg, Sweden

[6]Department of Clinical Neuroscience, Karolinska Institutet, Stockholm, Sweden

[7]Department of Medical Physics, Turku University Hospital, Turku, Finland

[8]Department of Radiology, University of Turku and Turku University Hospital, Turku, Finland

[9]Department of Pediatric Neurology, University of Turku and Turku University Hospital, Turku, Finland

[10]Department of Child Psychiatry, University of Turku and Turku University Hospital, Turku, Finland

Correspondence
Olli Rajasilta, FinnBrain Birth Cohort Study, Turku Brain and Mind Center, Institute of Clinical Medicine, University of Turku, Lemminkäisenkatu 2, 20520, Turku, Finland.
Email: operaj@utu.fi

Funding information
This study was supported by the Finnish Academy (HK), Hospital District of Southwest Finland State Research Grants (JJT, NMS, HK, LK), by Jane and Aatos Erkko Foundation (HK, LK), by the Signe and Ane Gyllenberg Foundation (NMS, HK), the Alfred Kordellin Foundation (JJT), Margaretha Foundation (OR), University of Turku Hospital District Foundation (OR, JJT), Maire Taponen Foundation (OR), Linnéa and Josef Carlssons Foundation (MB), and by the Maud Kuistila Memorial Foundation (OR).

Abstract

Resting-state functional magnetic resonance imaging (rs-fMRI) has been successfully used to probe the intrinsic functional organization of the brain and to study brain development. Here, we implemented a combination of individual and group independent component analysis (ICA) of FSL on a 6-min resting-state data set acquired from 21 naturally sleeping term-born (age 26 ± 6.7 d), healthy neonates to investigate the emerging functional resting-state networks (RSNs). In line with the previous literature, we found evidence of sensorimotor, auditory/language, visual, cerebellar, thalmic, parietal, prefrontal, anterior cingulate as well as dorsal and ventral aspects of the default-mode-network. Additionally, we identified RSNs in frontal, parietal, and temporal regions that have not been previously described in this age group and correspond to the canonical RSNs established in adults. Importantly, we found that careful ICA-based denoising of fMRI data increased the number of networks identified with group-ICA, whereas the degree of spatial smoothing did not change the number of identified networks. Our results show that the infant brain has an established set of RSNs soon after birth.

KEYWORDS

independent component analysis, neonate, resting-state fMRI, resting-state networks

1 | INTRODUCTION

Resting-state functional magnetic resonance imaging (rs-fMRI) provides a powerful tool for studying intrinsic brain organization, development of functional brain networks and effects of both environmental as well as endogenous factors on brain health and function (Graham et al., 2015; Zhang, Shen, & Lin, 2019). Based on the statistical dependencies in the spontaneous activity of different brain regions, a number of resting-state networks (RSNs) have been identified. Some of these networks are consistently reported in infants (Doria et al., 2010; Fransson et al., 2007; Gao, Alcauter, Elton, et al., 2015; Gao, Alcauter, Smith, Gilmore, & Lin, 2015; Kwon et al., 2015; Lin et al., 2008; Smyser et al., 2010) and adults (Rosazza & Minati, 2011; Smitha et al., 2017) despite differences in data acquisition and analysis techniques. Moreover, adult brain functional networks remain stable over time with little session-dependent variability (Gratton et al., 2018), permitting investigations into associations between functional brain organization and, for example, behavior or psychometric measures (Smith et al., 2015).

In adults, RSNs have been associated with multiple cognitive functions such as learning and memory consolidation, sensory and self-referential information processing and spontaneous thinking (Connoly et al., 2016; Dosenbach et al., 2007; Mary et al., 2017; Pan et al., 2016; Raichle, 2015; Reineberg, Andrews-Hanna, Depue, Friedman, & Banich, 2015; Tambini, Ketz, & Davachi, 2010). Recent rs-fMRI metrics have also shown great promise as potential biomarkers for a spectrum of central nervous system disorders in adults, including pain and mood disorders, as well as neurodegenerative diseases (Baggio et al., 2015; Brakowski et al., 2017; Khazaee, Ebrahimzadeh, & Babajani-Feremi, 2015; Zhao et al., 2017). Detectable differences are also seen in infant RSNs, as the consequences of, for example, preterm birth or have been found to associate to low family socioeconomic status (Gao, Alcauter, Elton, et al., 2015; Smyser & Neil, 2015). Further, rs-fMRI may also be implemented in exploring functional plasticity after training or injury, that is, how the brain reorganizes functional networks after cognitive task training or after a major structural lesion such as stroke (Gillebert & Mantini, 2013; Takeuchi et al., 2013, 2014).

Previous studies on preterm and term-born infants as well as 1- and 2-year-olds suggest that some of the identified RSNs are similar to those seen in adults, while others show distinct differences (Fransson et al., 2007; Gao, Alcauter, Elton, et al., 2015; Kwon et al., 2015; Lin et al., 2008; Smyser et al., 2010). Early RSNs in neonates encompass brain regions that later in life are known to support movement, auditory and sensory processing, whereas networks involved in cognitive functions, for example, the default mode network (DMN), salience network, and dorsal attention network tend to be underrepresented (Fransson et al., 2009; Gao, Alcauter, Elton, et al., 2015; Gao, Alcauter, Smith, et al., 2015; Gao et al., 2009). Specifically, neonatal correspondents of higher-order networks are often captured with incomplete or partial network topology, likely reflecting an immature intrinsic brain organization (Doria et al., 2010; Fransson et al., 2009; Gao, Alcauter, Elton, et al., 2015; Gao, Alcauter, Smith, et al., 2015; Gao et al., 2009; Lin et al., 2008). From a developmental point-of-view, many neonate RSNs have been reported as relatively large, containing lateralized intrahemispheric components (Fransson et al., 2009; Gao, Alcauter, Elton, et al., 2015; Gao, Alcauter, Smith, et al., 2015), whereas 1-year-old and older children have more bilateral and distributed functional connectivity patterns (Gao, Alcauter, Elton, et al., 2015; Gao, Alcauter, Smith, et al., 2015; Gao et al., 2011). Previously, up to 20 RSNs have been identified through seed-based connectivity analysis (SCA) and independent component analysis (ICA) studies in pre-term and term-born infants (Supplementary materials, Table S6). To our knowledge, no previous neonate studies have implemented "fsl_regfilt" or other ICA-based denoising strategies.

Many of these functional networks of the brain have been demonstrated to exhibit a hierarchical maturation pattern in which "early/primitive" networks achieve adult-like network topology earlier compared to "cognitive/higher-order" networks with lesser changes in the functional organization during the first year of life (Gao, Alcauter, Elton, et al., 2015; Gao, Alcauter, Smith, et al., 2015; Lin et al., 2008). In this context, adult-like topology is defined as increased connectivity strength within networks and the establishment of long-range functional connectivity (Gao, Alcauter, Elton, et al., 2015; Gao, Alcauter, Smith, et al., 2015; Lin et al., 2008). In the light of extant studies on the topic, a majority of these RSNs can be further classified into four groups based on their timing of maturation (Gao, Alcauter, Elton, et al., 2015; Gao, Alcauter, Smith, et al., 2015): (1) auditory/language and sensorimotor networks (AN/SM); at neonatal age, (2) medial occipital and occipital pole networks (V1/V2); by 3 months of age, (3) lateral visual/parietal and default-mode-networks (V3/DMN); by 12 months, and later on and (4) salience and bilateral frontopolar networks (SA/FPNs). In addition, changes in overall RSN topology and connectivity are accompanied by formidable reconfiguration of the functional cortical organization during development (Fair et al., 2009; Fransson, Aden, Blennow, & Lagercrantz, 2011; Gao, Alcauter, Elton, et al., 2015; Gao, Alcauter, Smith, et al., 2015; Zhang et al., 2019). In the current study, we characterize resting-state networks in ca. 3-week-old neonates by ICA and report how manually labeled ICA noise component removal affects the results.

2 | MATERIALS AND METHODS

This study was conducted in accordance with the Declaration of Helsinki, and it was approved by the Ethics Committee of the Hospital District of Southwest Finland (15.03.2011) §95, ETMK: 31/180/2011. Informed written consents were obtained from parents before MRI scans were conducted.

2.1 | Participants

Twenty-eight full-term born healthy infants (Table 1) were randomly recruited from the FinnBrain Birth Cohort Study to be included and participated in fMRI scans (scanned during the year 2015) (Karlsson et al., 2018). Exclusion criteria were interviewed during the recruitment phone calls and included perinatal complications of neurological involvement, less than 5 points in the 5 min Apgar, previously diagnosed central nervous system anomaly, gestational age at delivery less than 32 weeks, and birth weight less than 1,500 g. Out of 21 mothers, one reported having consumed a single cannabis and nicotine-containing cigarette once during the first trimester with concurrent use of alcohol. Four mothers reported having ingested alcohol during pregnancy, out of which three had done so 1–2 times per month for 1–3 standardized doses at a time and one had consumed 7–9 standardized doses less frequently than once per month during the pregnancy. All mothers ceased the use of alcohol or other substances upon receiving the knowledge of their pregnancy.

All scans were carried out during natural sleep at the gestation corrected age of 25.95 ± 6.69 days. To facilitate natural sleep, infants were fed with (breast) milk prior to the scanning session. Infants were protected from excess noise by dual protection, silicone putty earplugs (Mack's pillow soft silicone putty earplug), and earmuffs. Parents were allowed to stay in the scanner room throughout the scan. The scanning session was continuously monitored by research personnel through visual, microphone and loudspeaker contact to distinguish between states of sleep and wakefulness of the infant. Participating families were rewarded with a small thank you gift at the end of the session. The scans were performed on late afternoon hours, and some on noon hours during the weekends. The acquired anatomical (T1- and T2-weighted) images were screened by an experienced neuroradiologist for incidental findings. There were no incidental findings for the participants of the current study.

2.2 | MR image acquisition

Each infant underwent an MRI scanning session of the brain, including a 6-min resting-state fMRI sequence, conducted with Siemens Magnetom Verio 3T MRI scanner (Siemens Medical Solutions, Erlangen, Germany) equipped with a 12-element Head Matrix coil, allowing the use of Generalized Autocalibrating Partially Parallel Acquisition (GRAPPA) technique to accelerate acquisitions. Field-of-view (FOV) parameters were optimized for the replication of the scan in the future by linear alignment to anterior and posterior commissure line. The whole duration of the scanning protocol was 60 min, comprising of five major sequences in the following order: (1) Axial PD-T2-weighted TSE (Turbo Spin Echo), (2) Sagittal T1-MPRAGE (Magnetization Prepared Rapid Acquisition

TABLE 1 Demographics of subjects included in rs-fMRI analyses. Reported variables are based on previous recommendations (Pulli et al., 2018)

Variable	Whole sample ($N = 21$)	Boys ($N = 12$)	Girls ($N = 9$)
M ± SD (range)			
Age from birth (days)	26.00 ± 6.7 (13.0–40.0)	24.58 ± 6.08 (13.0–35.0)	27.78 ± 7.37 (19.0–40.0)
Age from term (days)	25.0 ± 6.1 (13.0–39.0)	24.0 ± 6.3 (13.0–35.0)	26.2 ± 6.1 (19.0–39.0)
Gestational age when born (weeks)	39.9 ± 1.1 (37.3–42.0)	39.8 ± 0.9 (38.1–41.1)	40.0 ± 1.4 (37.3–42.0)
Birth weight (g)	3,590.9 ± 339.4 (3085–4395)	3,562.5 ± 295.8 (3105–3980)	3,628.8 ± 405.9 (3085–4395)
Maternal age (years)	29.3 ± 4.5 (19–37)	29.1 ± 4.8 (19–37)	29.6 ± 4.3 (24–36)
Pre-pregnancy BMI (kg/m^2)	26.02 ± 3.9 (20.0–31.2)	25.92 ± 4.5 (20.0–34.4)	26.2 ± 3.4 (21.1–33.1)
Frequencies			
Maternal monthly income (€) (1=<500; 2 = 501–1,000; 3 = 1,001–1,500; 4 = 1,501–2,000; 5 = 2,001–2,500; 6 = 2,501–3,000; 7 = 3,001–3,500; 8 = 3,501–4,000; 9=>4,000)	2/2/2/10/4/0/0/1/0	1/0/2/5/4/0/0/0/0	1/2/0/5/0/0/0/1/0
Race/Ethnicity (Caucasian/Other)	21/0	12/0	9/0

Gradient Echo), (3) GRE field mapping, (4) DTI images, and (5) a 6-min duration EPI (Echo-planar imaging) sequence. The rs-fMRI sequence consisted of 42 slices with a voxel size of 3.0 × 3.0 × 3.0 mm, TR of 2,500 ms, TE of 30 ms, FOV of 216 × 216 mm, and flip-angle (FA) of 80 degrees. Additionally, Fat Saturation technique was used to reduce artifacts. Bandwidth (Bw) was set to 1,310 Hz/Px for improved signal-to-noise ratio. A total of six subjects were excluded from the study due to excess motion artifacts and one due to motion and premature termination of the scanning. In the excluded subjects, there was motion larger than 3 mm in multiple time points and it was clear that no usable data were available from these excluded participants.

2.3 | Image preprocessing

The generated images of 21 subjects were processed with FEAT (FMRI Expert Analysis Tool), part of the MELODIC toolbox of Oxford Center for Functional MRI of the Brain Software Library (FSL), for MCFLIRT motion correction (Jenkinson, Bannister, Brady, & Smith, 2002), interleaved slice timing correction using Fourier-space time-series phase-shifting, removal of non-brain voxels with brain extraction toolbox BET (Smith, 2002), spatial smoothing using Gaussian kernel values of FWHM 5 mm, grand-mean intensity normalization of the entire 4D data set by a single multiplicative factor, and high-pass temporal filtering (Gaussian-weighted least-squares straight line fitting with $\sigma = 100$ s). Registration/normalization was performed to a brain extracted UNC infant T2 template (Shi et al., 2011) with linear full search and 12 degrees of freedom (DOF) using FLIRT (FMRIB's Linear Image Registration Tool) (Jenkinson et al., 2002; Jenkinson & Smith, 2001). We would like to note that using individual structural MR images as a waypoint to standard space registration is the standard for adult data. However, registrations for the current data frequently failed with this approach, more specifically, at the outlines of the brain and the ventricles. Registrations directly to the infant UNC template space were exceedingly more successful than via individual structural T1 or T2 weighed images, and thus chosen for the preprocessing of the current data set.

2.4 | Independent component analysis

IC analysis was carried out using probabilistic ICA (Beckmann & Smith, 2004, 2005; Hyvärinen, 1999) as implemented in MELODIC (Multivariate Exploratory Linear Decomposition into Independent Components) Version 3.14. Subject-level ICA was utilized for optimization and quality control of the preprocessing step for group-level ICA, as well as separating noise and signal components for manual denoising. Subject-level ICA yielded 24–45 components per subject, out of which on average 52.7% (35.0%–82.8%) were classified as noise components.

For noise removal, we identified and labeled the components as a potential signal, noise or mixture components as per previously published criteria (Griffanti et al., 2017). Labeling of components was first performed independently by two investigators (OR and JJT) followed by a joint decision on final labeling. We then implemented "fsl_regfilt" with default settings (unique variance clean-up) for removing noise components from subject-level-IC-analysis without causing discontinuation of rs-fMRI time series.

We then ran two versions of the group ICA. The preprocessed and preprocessed & denoised rs-fMRI data sets were then entered into group-level analyses. Group-level ICA with multi-session temporal concatenation was used to delineate global functional resting-state networks. Masking of non-brain voxels, voxel-wise de-meaning of the data and normalization of the voxel-wise variance were applied to the input data. ICA maps were thresholded at 0.5. The number of components was optimized using Laplace approximation to the Bayesian evidence of the model order (Beckmann & Smith, 2004). Results of the group-ICA correspond to statistically independent components, that is, estimates of functional RSNs.

2.5 | Note on the protocol optimization

Since an infant brain is about 1/3 of adult brain volume, the voxel dimension should be scaled to $(1/3)^{1/3}$ as compared to adult studies. However, this was unfeasible for the current study and would have had a dramatic impact on the MRI signal-to-noise ratio. We thus tested the sensitivity of our analysis to spatial smoothing to exclude that spatial smoothing did not strongly affect the results, as well as resampling resolution parameters and compared results using a fixed number of components (20–60) as compared to automatic dimensionality estimation. We are confident that the best results were obtained with the used procedures. Additionally, we included a group-ICA model without manual denoising to highlight the extent to which manual denoising affects the ICA maps as well as alternative manually denoised group-ICA run and limited dimensionality runs of 20, 25, 30, and 35 components in the supplemental material, to accentuate the robustness of our findings. Further, we performed a sensitivity analysis with four subjects excluded that were exposed to alcohol and/or illicit substances during gestation. We report the results of the sensitivity analysis in the supplementary materials. No significant changes were observed that could be attributed to prenatal alcohol and/or illicit substance exposure.

3 | RESULTS

Group-ICA without manual denoising yielded 20 components, of which 13 were identified as potential RSNs (Table 2). Group-ICA with manual denoising produced 61 total components, of which 44 were identified as potential RSNs (Table 2). The naming of components is based on anatomical location rather than functional regions, with reserve

TABLE 2 Components identified by group ICA

Group-level ICA without denoising—found RSNs (% of explained variance)	
N1—Frontocingular network (5.55%)	N8—Right parietotemporal network (5.01%)
N2—Bilateral motor network (5.44%)	N9—Bilateral posterior cerebellar network (4.95%)
N3—Bilateral anterior sensorimotor network (5.41%)	N10—Left temporoparietal network (4.89%)
N4—Bilateral primary visual network (5.35%)	N11—Bilateral insular/temporal cortices and posterior cingulate cortex (4.89%)
N5—Network encompassing brainstem and thalamus (5.24%)	N12—Left frontoparietal network (4.67%)
N6—Bilateral posterior parietal network (5.10%)	N13—Right frontoparietal network (4.54%)
N7—Bilateral posterior sensorimotor network (5.04%)	
Denoised Group-level ICA—found RSNs (% of explained variance)	
Cerebellar components	**Temporal components**
R1—Bilateral posterior cerebellar network (1.78%)	R2—Bilateral anterior temporal network with right prominence (1.76%)
R40—Left anterolateral cerebellar network (1.59%)	R18—Left temporal pole/anterior temporal network (1.67%)
R44—Anterior cerebellar network encompassing cerebellar peduncles (1.48%)	R30—Left posterior temporal network (1.62%)
Basal ganglia, brainstem and thalamic components	R34—Left lateral temporal network (1.61%)
R3—Bilateral basal ganglia network (1.74%)	R35—Right lateral temporal network (1.61%)
R10—Bilateral thalamic network (1.71%)	**Temporoparietal components**
R26—Brainstem network (1.65%)	R20—Right temporoparietal network (1.66%)
R37—Medial cerebellar and brainstem network (1.60%)	R38—Right lateral temporoparietal network (1.60%)
Insular components	R39—Left temporoparietal network (1.60%)
R4—Bilateral insular network with right prominence (1.74%)	**Parietal components**
R13—Bilateral insular network with left prominence (1.70%)	R12—Bilateral posteromedial parieto-occipital network (1.70%)
Occipital/visual components	R15—Right posterolateral parietal network (1.69%)
R6—Medial visual network (1.73%)	R31—Left posterolateral parietal network (1.62%)
R8—Bilateral lateral occipital network with left prominence (1.71%)	R32—Bilateral superior medial parietal network (1.62%)
R16—Primary visual network (1.68%)	**Frontal components**
R19—Right lateral occipital network (1.66%)	R28—Right frontal network (1.63%)
Motor components	R42—Left frontal network (1.58%)
R17—Bilateral anterior motor network (1.67%)	**Cingulate components**
R21—Bilateral inferior frontal gyri network (1.66%)	R9—Dorsal default-mode-network encompassing precuneus and posterior cingulate cortex (1.71%)
R22—Bilateral ventral supplementary motor network with somatosensory medial area signal (1.66%)	R24—Anterior cingulate cortex network (1.65%)
R23—Bilateral medial supplementary motor network with left somatosensory area signal (1.66%)	**Prefrontal components**
Sensorimotor components	R14—Bilateral prefrontal network encompassing lateral and medial areas (1.69%)
R5—Bilateral anterior sensorimotor network (1.73%)	R25—Bilateral medial prefrontal network (1.65%)
R7—Right sensorimotor network, lateral-medial orientation (1.73%)	R27—Bilateral lateral prefrontal network (1.63%)
R11—Bilateral posterior sensorimotor network (1.71%)	R33—Right lateral prefrontal network (1.61%)
R29—Left sensorimotor network, ventral-dorsal orientation (1.63%)	R41—Bilateral ventrolateral prefrontal network (1.58%)
R36—Bilateral superior sensorimotor network (1.61%)	R43—Anterior prefrontal network (1.56%)

to components that were identified as RSNs based on the previous literature (noting that there is considerable variability in naming similar components in previous literature). Figures 1 and 2 show RSN spatial maps captured by group-ICA without and with manual denoising, respectively. The respective power spectral distributions of these group-ICA

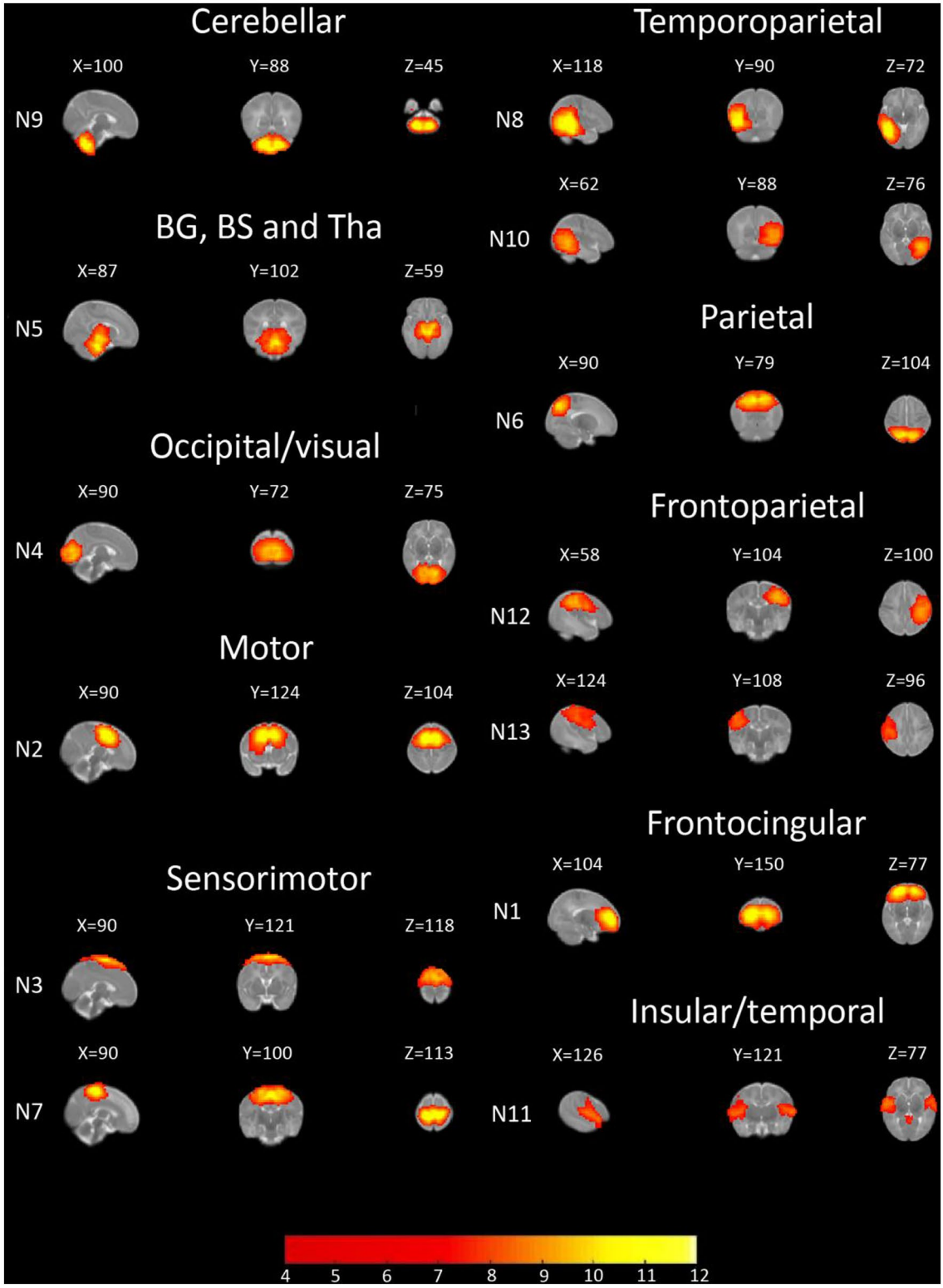

FIGURE 1 Components in naturally sleeping neonates ($N = 21$) identified by group-ICA without manual denoising on sagittal, coronal, and axial slices from left to right. Image intensity threshold is shown in the color bar at the right lower corner. The images are shown in the radiological convention on the UNC neonate template

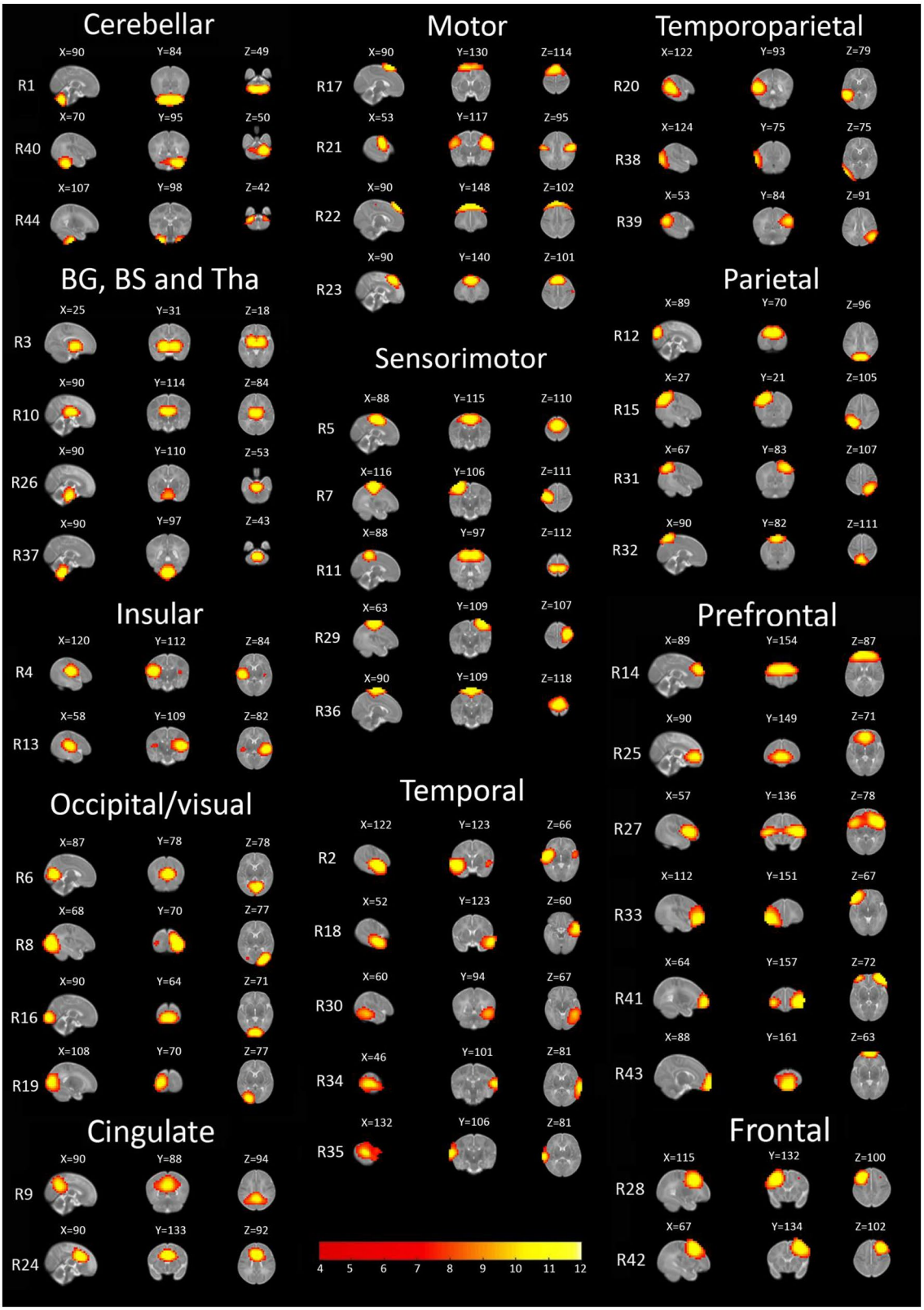

FIGURE 2 Components in naturally sleeping neonates ($N = 21$) identified by group-ICA with manual denoising on sagittal, coronal, and axial slices. Image intensity threshold is shown in the color bar at the right lower corner. The images are shown in the radiological convention on the UNC neonate template

decompositions are displayed in Figure 3. RSN spatial maps and power spectral distributions of manually denoised group-ICA run with 3 mm FWHM spatial smoothing and limited dimensionality runs of 20, 25, 30, and 35 components are available in the supplemental material.

With group-ICA without denoising, we could identify 10/18 corresponding components to previously published RSNs (Supplementary materials, Table S6). These included the frontocingular network (N1), bilateral motor network (N2), bilateral anterior and posterior sensorimotor networks (N3, N7), bilateral visual network (N4), brainstem and thalamic network (N5), right and left temporoparietal networks (N8, N10), bilateral posterior cerebellar network (N9), and a network encompassing a bilateral insular-temporal-posterior

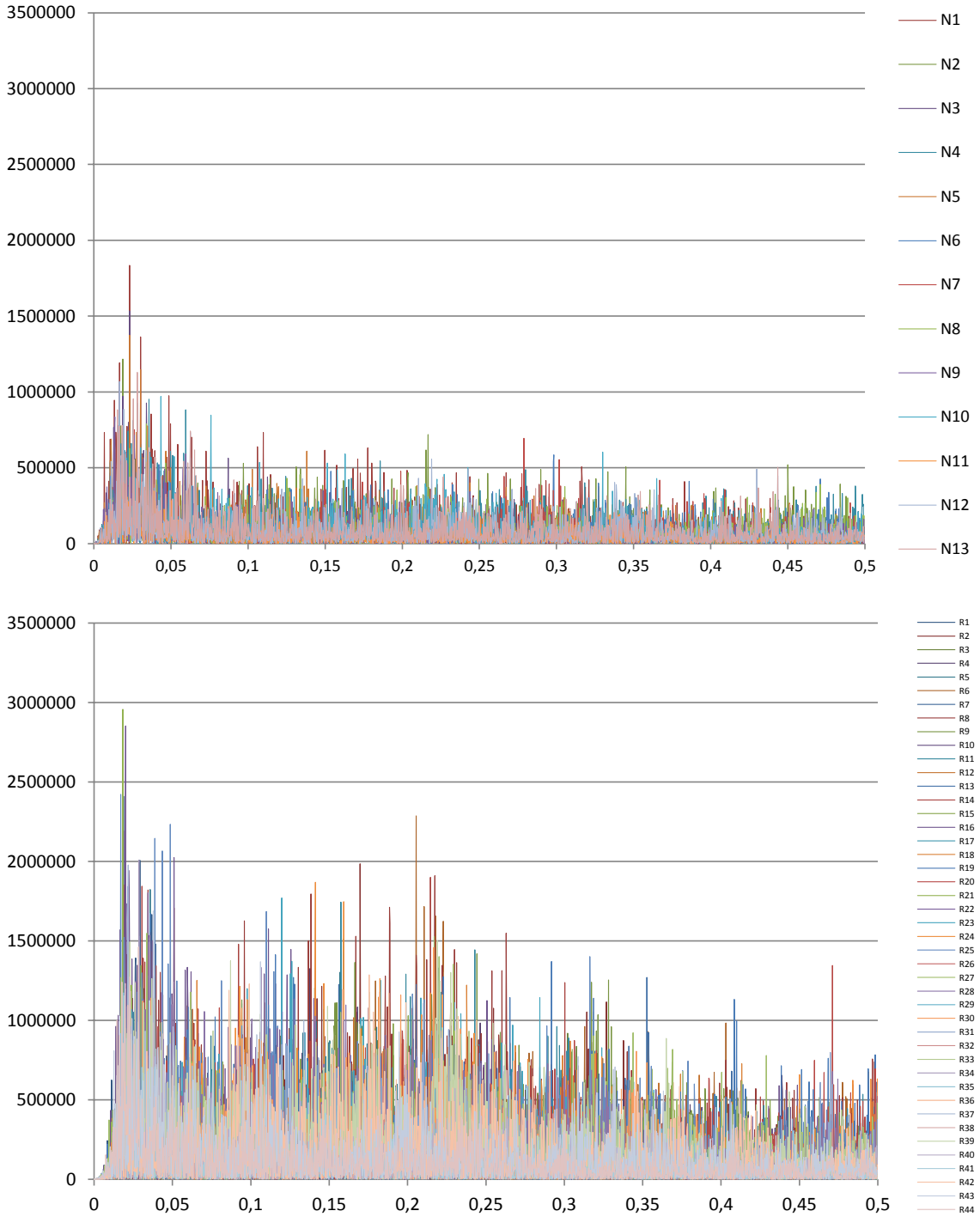

FIGURE 3 Color-coded power spectra of included components from group-ICA without denoising (upper image) and from manually denoised group-ICA run (lower image). Horizontal axis denotes frequencies as f/10 Hz. Vertical axis denotes power amplitude

cingulate network (N11). RSN correlates of N12-13 have not been reported in previous neonate studies; however, anatomically these functional areas correspond to the unilateral parietal-frontal networks and may reflect an early form of dorsal parietal attention network (Gao et al., 2013). Out of the total 13 signal components, only N11 exhibited bilateral functional connectivity, whereas the remaining RSNs displayed typical localized patterns of signal commonly seen in neonate scans (Doria et al., 2010; Fransson et al., 2007, 2009, 2011; Lee, Morgan, Shroff, Sled, & Taylor, 2013; Lin et al., 2008; Smyser et al., 2010).

The identified independent components generated after manual denoising sharing similar spatial characteristics with previously reported networks (Supplementary materials, Table S6), included posterior (R1) and left anterolateral cerebellar (R40); bilateral basal ganglia (R3); thalamic (R10); brainstem (R26 and R37); bilateral insular with right/left prominence (R4, R13); primary (R16), medial (R6) and lateral (R8, R19) visual; bilateral inferior frontal gyri (R21); anterior (R5), posterior (R11) and superior (R36) sensorimotor; anterior temporal (R2, R18); right (R15) and left (R31) posterolateral parietal; dorsal (R9) and ventral (R25) default-mode; anterior cingulate cortex (R24); medial and lateral prefrontal (R14); and lateral prefrontal (R41) networks (Table 2).

Previously unreported independent components comprised of the bilateral anterior motor (R17), bilateral ventral (R22) and medial supplementary motor (R22-23); right (R7) and left sensorimotor (R29); left (R34) and right (R35) lateral temporal; temporo-parieto-occipital (R38); left temporoparietal (R39); posteromedial parieto-occipital (R12); superior medial parietal (R32); right (R28) and left (R42) frontal; bilateral lateral prefrontal (R27); right lateral prefrontal (R33); and anterior prefrontal (R43) networks (Table 2).

We briefly describe the identified components with regard to their anatomical location in an approximate dorsal to ventral order.

Cerebellar, brain stem and subcortical components included posterior bilateral cerebellar (R1), left cerebellar (R40), and anterolateral cerebellar peduncles (R44). Deep nuclei and brainstem components comprised of anterior basal ganglia (R3), bilateral thalamic (R10), and two separate spatiotemporal configurations of brainstem signal (R26 and R37). These components showed great spatial map similarity as compared to previous studies' corresponding reported RSNs (Supplementary materials, Table S6).

Occipital/visual components were captured in four separate parts: Primary visual area (R16), medial visual area (R6), right lateral visual area (R19), and left lateral visual area (R8). Primary and medial visual areas presented with an analogous manner to previous studies (Supplementary materials, Table S6), while the lateral visual components exhibited slightly diverging spatial patterns with the left lateral visual component (R8) exhibiting minor bilateral spatial distribution. Components involved in visual processing were captured here without discrepancy regarding their functional development (Gao, Alcauter, Elton, et al., 2015; Gao, Alcauter, Smith, et al., 2015), with primary and medial visual areas resembling more mature spatial topology in contrast to lateral visual areas.

Temporal lobe components in the left anterior temporal/temporal pole region (R18), left posterior temporal region (R30), left and right lateral temporal regions (R34-35, respectively) emerged as unilateral networks. The right anterior temporal region (R2) component exhibited a bilateral spatial pattern. Prior studies focusing on networks involved in auditory processing and language development in older infants have linked medial and superior temporal cortices with these functions (Dick, Solodkin, & Small, 2010; Emerson, Gao, & Lin, 2016) with overlapping areas seen in components R2, R18, R34-35. While neonate auditory systems are limited in their ability to comprehend language, there is evidence of differentiation of sound characteristics (Bendixen et al., 2015; Telkemeyer et al., 2009) and distinguishing familiar sound sources (Beauchemin et al., 2011), for example, maternal voice causes distinct auditory processing compared to a strangers voice. These findings may reflect the development of auditory networks during gestation and soon after birth. Insular cortex components (R4 and R13 for left and right, respectively) both exhibited robust unilateral signal with a minor spatial distribution of the signal to the contralateral homologous area, but no distal distribution of signal to previously well-described functional regions in older infants (Alcauter, Lin, Smith, Gilmore, & Gao, 2015).

Temporoparietal components included right (R20) and left (R39) temporoparietal junctional areas. In older infants, the functional areas that overlap with components R20, R30, and R39 have been associated with language development (Emerson et al., 2016) and therefore, these components may be the neonatal precursors of such functional networks. Our group-ICA also captured a component with posterior temporo-parieto-occipital involvement (R38), which has similar spatial characteristics as V3 found in neonates (Gao, Alcauter, Elton, et al., 2015), but emerged without a homologous contralateral counterpart.

Parietal lobe components appeared as each other's spatially homologous counterparts**,** right (R15) and left posterolateral parietal areas (R31). These components resemble the dorsal components of the left and right frontopolar or executive control networks (Gao, Alcauter, Elton, et al., 2015; Gao, Alcauter, Smith, et al., 2015) in their spatial distribution of the signal. Two of the components enveloping the superior (R32) and inferior (R12) medial aspects of the parietal region have not been previously delineated in neonates. In adults, the corresponding functional areas have been linked to visuomotor and visuospatial functions (Ray et al., 2013).

Motor and sensorimotor components in inferior frontal gyri (R21) and anterior motor cortex (R17) emerged as bilateral components. A supplementary motor area was captured in two converging spatial configurations with R22 including lateral and more superior areas and R23 with medial and central areas. Notably, both of these components exhibit slight distal spatial distribution emerging as few voxel signal clusters in the sensorimotor domains near the post- and precentral gyri. The distal spatial distribution of R22 appears medially and that of R23 localizing to left lateral parts of the post- and precentral gyri. Sensorimotor components with bilateral spatial configurations included anterior (R5), posterior (R11), and superior (R36) regions. These components have been previously documented in neonates (Supplementary materials, Table S6). Lateralized spatial patterns were found in components enveloping right (R7) and left (29) pre- and postcentral gyri, albeit with slightly diverging spatial configurations. Emergence of sensorimotor and motor networks in multiple separate components suggests diverging information processing (Fransson et al., 2011; Gao, Alcauter, Smith, et al., 2015).

Prefrontal components shared spatial patterns with previously published RSNs in the bilateral medial and lateral aspects of the prefrontal cortex (PFC) (R14) (Fransson et al., 2009) and bilateral ventrolateral PFC (R41) (Gao, Alcauter, Elton, et al., 2015; Gao, Alcauter, Smith, et al., 2015; Smyser et al., 2010). We found no prior evidence of neonate RSNs that conveyed to the spatial distribution patterns of components involving bilateral lateral PFC (R27), right lateral PFC (R33), or anterior medial PFC (R43). Of the unilateral frontal components, a contralateral counterpart was found for R28, enveloping a large section of the frontal lobe and premotor area (R42). In adults, these prefrontal and frontal regions have been associated with various higher-order cognitive functions, such as goal-driven behavior (Marek & Dosenbach, 2018) and reward processing (Huckins et al., 2019), attention and working memory (Lara & Wallis, 2015) and mimicry to others' behavior (Wang, Ramsey, & Hamilton, 2011). It is thus interesting that such components are observable in neonates, although their functions at this age are admittedly unknown.

Cingulate components included precuneal and posterior cingulate cortex (PCC) (R9) and anterior cingular cortex (ACC) (R24). Component R24 consisted of anterior cingulate cortex as a local cluster with no apparent distributed spatial characteristics. Similar patterns of ACC signaling have been demonstrated in previous neonate studies (Lee et al., 2013; Smyser et al., 2010). A correspondent to the DMN may has been captured in two separate components (R9 and R25), displaying incomplete network spatial topology as compared to older infants and adults (Gao, Alcauter, Elton, et al., 2015; Gao, Alcauter, Smith, et al., 2015; Wylie et al., 2014). Component R25 demonstrated robust medial PFC and ACC spatial features, and may correspond to the ventral DMN, while component R9 coincides with the dorsal DMN. This pattern has been reported in prior studies (Gao, Alcauter, Elton, et al., 2015; Gao, Alcauter, Smith, et al., 2015; Wylie et al., 2014). A recent study delineated the development of DMN from 2 weeks to 2 years of age (Gao et al., 2009), suggesting not just incomplete network spatial topology with merely 6 out of 13 coinciding regions compared between neonates and 1-year-olds, but also the dispersion of signal to separate ICA captured spatiotemporal components.

4 | DISCUSSION

In this study, we found evidence for a set of RSNs previously reported in neonate SCA and ICA rs-fMRI studies, comprising of visual, auditory, thalamic, basal ganglia, cerebellar and brainstem, insular, sensorimotor, motor, default-mode, and prefrontal networks. Furthermore, with careful manual denoising, previously unreported networks were found in the frontal, parietal, and temporal lobes.

Group-ICA with manual denoising unveiled both previously delineated as well as unpublished RSN components. The majority of previously unpublished components appear to describe various interactions between spatial configurations of frontal, temporal, and parietal lobe areas. This is in line with previous findings suggesting that distributed networks such as the DMN are most susceptible to head motion, and this may explain why they are not captured in the analysis without denoising (Kim, Vaj Dijk, Libby, & Napadow, 2014; Power, Barnes, Snyder, Schlaggar, & Petersen, 2012). With comparison to data that were not manually denoised, many components were likely divided into subcomponents with overlapping spatial, but not temporal configurations when using manual denoising. A similar phenomenon has been observed in large adult data sets (Ray et al., 2013). There is also some evidence that as ICA dimensionality increases, major networks become subdivided into separate functionally feasible independent components (Pamilo et al., 2012).

Our results demonstrate clear differences in neonate as compared to canonical RSNs found in older infants and adults (Supplementary materials; Table S6; Rosazza & Minati, 2011; Smitha et al., 2017), in the sensorimotor, motor, temporal, temporoparietal, and prefrontal RSNs. In line with previous studies, our estimates of RSN spatial maps in the neonate appear largely localized with little distributed connectivity. These divergences are likely related to different functionalities of the networks in the sleeping neonate as well as fundamental differences in the global network organization. The functional hubs of neonate cortical networks have been reported to be located mainly in the homomodal primary sensorimotor, auditory and visual systems and only to a small extent in higher-order associative cortices (Fransson et al., 2011; Gao, Alcauter, Smith, et al., 2015). In contrast,

functional cortical hubs in children older than 12 months and adults include higher-order brain regions, such as the posterior cingulate gyrus, precuneus, and prefrontal areas (Gao, Alcauter, Smith, et al., 2015). This shift is majorly timed to take effect during the first two years of life, emphasizing early life to be a critical, dynamic, period in functional network architecture development (Gao, Alcauter, Smith, et al., 2015; Gao et al., 2011). These prominent changes in RSN topology coincide with neurobiological development such as myelination (Thomas et al., 2000; Volpe, 2008) and synaptic pruning (Andersen, 2003; Bourgeois, 1997; Knickmeyer et al., 2008). In addition, it should be noted that electrographic studies fundamentally differ in generative mechanisms of resting-state activity in neonates and adults: In neonates, resting-state activity appears largely driven by the sensory periphery, whereas in adults thalamocortical connections dominate (Colonnese & Khazipov, 2012). This distinction has been interpreted to reflect different functional purposes such as circuit formation as opposed to attention. Finally, comparisons of infant and adult RSNs are complicated by the large differences in brain structure, vascular physiology, and function as well as the differences between infant sleep and adult wakefulness (Mitra et al., 2017).

Interestingly, emerging evidence suggests that rs-fMRI signal fluctuations related to brain function are not limited to <0.1 Hz frequencies as commonly assumed (Alcauter, Lin, Smith, Goldman, et al., 2015; Kalcher et al., 2014; Niazy, Xie, Miller, Beckmann, & Smith, 2011; Smith-Collins, Luyt, Heep, & Kauppinen, 2015) and this may carry important implications for studies on brain development. To our knowledge, only one study (Alcauter, Lin, Smith, Goldman, et al., 2015) has investigated neonate RSN power spectral densities (PSDs) and their correlations with cognitive performance. The results of that study suggested that a right-ward shift in PSD peak frequency from lower to higher frequencies from neonatal age to adulthood is associated with better performance of investigated cognitive networks. Similar follow-up settings will provide a fruitful venue for future studies in our study population as well as in other cohorts. In line with their findings, we found a PSD peak frequency of 0.01–0.075 Hz in neonate RSNs (Figure 3). With manual denoising, there were also prominent power bands at 0.08–0.28 Hz. Irrespective of denoising, both analyses also demonstrated continuous low intensity power oscillation (<0.5 Hz) that was likely caused by the inability of fMRI to properly sample higher frequencies (Lowe, Mock, & Sorenson, 1998; Power et al., 2012). In sum, the higher frequencies may carry important information on brain development (Alcauter, Lin, Smith, Goldman, et al., 2015; Kalcher et al., 2014; Niazy et al., 2011; Smith-Collins et al., 2015). Future studies upon this important topic should take into account that also PSDs of infant RSNs are strongly affected by denoising. Recent work on sampling rates in adults (Huotari et al., 2019) suggests only minimal effects of variable TR values from 0.1 to 3.0 s on ICA generated RSN spatial estimates as defined within low-frequency oscillations (<0.1 Hz).

As compared to previous similar studies (Supplementary materials, Table S7), this current work utilized similar image acquisition parameters including MR field strength, TR/TE values, and voxel dimensions. We used a higher number of slices (42) to permit identical image acquisition sequence usage in follow-up studies. Additionally, Fat Saturation technique was used to mitigate artifacts, which inevitably increases TR by 0.6 s. Comparable methodology to previous studies was also used in the preprocessing phase including the implementation of high-pass temporal filtering and spatial smoothing FWHM kernel values. In contrast to most previous neonate rs-fMRI studies, in this study, the rs-fMRI data were directly transformed to UNC2 neonate T2 template space without subject-specific structural T1/T2 co-registration step. This was due to many of our subjects lacking pristine quality T2-weighted images and the use of both T1 and T2-weighted images as an inter-subject mixture created unwanted variance in the preprocessing phase, resulting in reduction in accuracy of registration and quality of ICA components as compared to group-ICA runs without structural co-registration to individual T1/T2 weighted images.

As a first for neonate rs-fMRI studies, we also implemented "fsl_regfilt" for manual motion removal. This technique involves manually identifying and labeling unwanted noise components derived from subject-level IC analyses. These components are removed after labeling via a simple algorithm in FSL, generating denoised subject-level rs-fMRI data sets to be used in group-level analyses. A clear advantage of "fsl_regfilt" to other denoising paradigms is the better conservation of neural-related signal as opposed to noise volume "scrubbing" and linear regression of extra-neural signal techniques, which tend to remove wanted signal in the process of removing noise. Linear regression techniques also require the masking of non-brain voxels which easily leads to overlapping with parenchymal voxels due to small areas of interest, affecting the consecutive spatial estimation of filtering. Furthermore, "fsl_regfilt" does not cause the discontinuation of rs-fMRI time series, further increasing the spatiotemporal estimations of ICA components. Using probabilistic dimensionality estimation coupled with "fsl_regfilt," the total amount of generated components and signal components increased by 3.05- and 3.38-fold, respectively, in our data set. As motion has complex inter-artifactual global effects on the spatiotemporal dimensions of acquired MR-signal with the emphasis on increasing local connectivity patterns (Power et al., 2012), removing noise components prior to group-level analyses increases the statistical independency for all generated components. This permits ICA algorithms to couple spatial and temporal information with improved statistical accuracy to generate better estimates for

components and reveal spatially overlapping sub-networks. A major disadvantage of "fsl_regfilt" is the task of labeling each subject-level component accurately, which is a strenuous task, especially with larger samples. Denoising larger samples manually introduce more investigator related variability to selecting noise components, which may affect results. It is unclear whether "fsl_regfilt" performs well with samples largely corrupted by motion; in these samples, most components likely comprise of mixture of variable quantity of noise and signal. Removing these mixture components results in the loss of neural signal to be used in group-level analyses, while including them leads to motion corruption of group-level analyses, furthering the loss of already weak distal connectivity patterns in neonates and therefore poorer estimates of RSN spatial maps. It may be beneficial for future studies with considerable motion corruption to couple "fsl_regfilt" with another denoising paradigm dedicated to removing motion-related noise to improve component estimates. Future studies may also benefit from different denoising algorithms (e.g., automatic ICA denoising with and without study-specific training data) to improve cross-study reliability (Griffanti et al., 2014; Pruim et al., 2015; Salimi-Khorshidi et al., 2014).

5 | LIMITATIONS

A larger sample would likely have allowed more precise component estimates (Gao et al., 2014; Mueller et al., 2013; Xu et al., 2019). Recently proposed optimized sequences for infant scans that were not available for while our data were collected (Goksan et al., 2017) are important to take note of in future studies. We had to balance between the time constraints of the whole imaging session, which limited the total acquisition time available to rs-fMRI, the TR, the voxel size with regard to image quality. The voxel dimensions of $3.0 \times 3.0 \times 3.0$ mm correspond to rougly $4.5 \times 4.5 \times 4.5$ mm in adult scans and this poses important limitations to our analyses. Nevertheless, our data are comparable to other published data sets (Supplementary materials, Tables S6 and S7). Although infant sleep seems to more closely resemble adult wakefulness than adult sleep in terms of RSN connectivity (Horovitz et al., 2009; Larson-Prior et al., 2009; Tagliazucchi et al., 2013), as well as exhibiting significant differences in thalamic BOLD-signal propagation patterns (Mitra et al., 2017), one major shortcoming in the current study is the lack of control over sleep states.

6 | CONCLUSIONS

We found evidence of previously unreported neonatal RSNs that demonstrate distinguishable spatiotemporal characteristics and localized them to prefrontal, temporal, and parietal regions, as well as replicated former findings of neonate RSN presence shortly after birth. The majority of the previously unreported ICA components emerged as spatially overlapping sub-components of previously delineated neonate RSNs. Furthermore, we report that denoising neonate rs-fMRI data increased the number of identifiable RSN components in group-ICA and hope the reported set of functional networks serves as a benchmark for future studies.

CONFLICT OF INTEREST

None.

AUTHOR CONTRIBUTIONS

JJT, MB, NMS, HK, and MB planned and/or funded the MR measurements. JS planned and implemented the image acquisition parameters. JJT and SL collected the imaging data. OR and JJT planned the analytical approach and performed the data analyses. HM and SH aided in the analysis planning and interpretation. RP provided neuroradiological expertise for screening the acquired MRI images for incidental findings. HK and LK established the cohort and built the infrastructure for carrying out the study. All authors participated in writing the manuscript and accepted the final version.

DATA AVAILABILITY STATEMENT

The Finnish law and ethical permissions do not allow the sharing of the data used in this study.

ORCID

Olli Rajasilta https://orcid.org/0000-0002-7524-8217

REFERENCES

Alcauter, S., Lin, W., Smith, J. K., Gilmore, J. H., & Gao, W. (2015). Consistent anterior–posterior segregation of the insula during the first 2 years of life. *Cerebral Cortex*, *25*(5), 1176–1187.

Alcauter, S., Lin, W., Smith, J. K., Goldman, B. D., Reznick, J. S., Gilmore, J. H., & Gao, W. (2015). Frequency of spontaneous BOLD signal shifts during infancy and correlates with cognitive performance. *Developmental Cognitive Neuroscience*, *12*, 40–50.

Andersen, S. L. (2003). Trajectories of brain development: Point of vulnerability or window of opportunity? *Neuroscience and Biobehavioral Reviews*, *27*, 3–18.

Baggio, H. C., Segura, B., Sala-llonch, R., Marti, M. J., Valldeoriola, F., Compta, Y., … Junque, C. (2015). Cognitive impairment and resting-state network connectivity in Parkinson's disease. *Human Brain Mapping*, *36*(1), 199–212.

Beauchemin, M., González-Frankenberger, B., Tremblay, J., Vannasing, P., Martinez-Montez, E., Belin, P., … Lassonde, M. (2011). Mother and stranger: An electrophysiological study of voice processing in newborns. *Cerebral Cortex*, *21*(6), 1705–1711.

Beckmann, C. F., & Smith, S. M. (2004). Probabilistic independent component analysis for functional magnetic resonance imaging. *IEEE Transactions on Medical Imaging*, *23*(2), 137–152. https://doi.org/10.1109/TMI.2003.822821

Beckmann, C. F., & Smith, S. M. (2005). Tensorial extensions of independent component analysis for multisubject FMRI analysis. *NeuroImage*, *25*(1), 294–311. https://doi.org/10.1016/j.neuroimage.2004.10.043

Bendixen, A., Háden, G. P., Nèmeth, R., Farkas, D., Török, M., & Winkler, I. (2015). Newborn infants detect cues of concurrent sound segregation. *Developmental Neuroscience*, *37*(2), 172–181. https://doi.org/10.1159/000370237

Bourgeois, J. P. (1997). Synaptogenesis, heterochrony and epigenesist in the mammalian neocortex. *Acta Paediatrica Supplement*, *422*, 27–33.

Brakowski, J., Spinelli, S., Dörig, N., Bosch, O. G., Manouli, A., Holforth, M. G., & Seifritz, E. (2017). Resting state brain network function in major depression—Depression sympatomology, antidepressant treatment effects, future research. *Journal of Psychiatric Research*, *92*, 147–159.

Colonnese, M., & Khazipov, R. (2012). Spontaneous activity in developing sensory circuits: Implications for resting state fMRI. *NeuroImage*, *62*(4), 2212–2221.

Connoly, J., McNulty, J. P., Boran, L., Roche, R. A., Delany, D., & Bokde, A. L. (2016). Identification of resting state networks involved in executive function. *Brain Connectivity*, *6*(5), 365–374.

Dick, A. S., Solodkin, A., & Small, S. L. (2010). Neural development of networks for audiovisual speech comprehension. *Brain and Language*, *114*(2), 101–114.

Doria, V., Beckmann, C. F., Arichi, T., Merchant, N., Groppo, M., Trukheimer, F. E., … Edwards, A. D. (2010). Emergence of resting state networks in the preterm human brain. *Proceedings of the National Academy of Sciences of the United States of America*, *107*(46), 20015–20020.

Dosenbach, N. U., Fair, D. A., Miezin, F. M., Cohen, A. L., Wenger, K. K., Dosenbach, R. A., … Petersen, S. E. (2007). Distinct brain networks for adaptive and stable task control in humans. *Proceedings of the National Academy of Sciences of the United States of America*, *104*, 11073–11078. https://doi.org/10.1073/pnas.0704320104

Emerson, R. W., Gao, W., & Lin, W. (2016). Longitudinal study of the emerging functional connectivity asymmetry of primary language regions during infancy. *The Journal of Neuroscience*, *36*(42), 10883–10892.

Fair, D. A., Cohen, A. L., Power, J. D., Dosenbach, N. U., Church, J. A., Miezin, F. M., … Petersen, S. E. (2009). Functional brain networks develop from a "local to distributed" organization. *PLoS Computational Biology*, *5*(5), e1000381.

Fransson, P., Aden, U., Blennow, M., & Lagercrantz, H. (2011). The functional architecture of the infant brain as revealed by resting-state fMRI. *Cerebral Cortex*, *21*(1), 145–154.

Fransson, P., Skiöld, B., Engström, M., Hallberg, B., Mosskin, M., Åden, U., … Blennow, M. (2009). Spontaneous brain activity in the newborn brain during natural sleep—An fMRI study in infants born at full term. *Pediatric Research*, *66*(3), 301–305.

Fransson, P., Skiöld, B., Horsch, S., Nordell, A., Blennow, M., Lagercrantz, H., & Åden, U. (2007). Resting-state networks in the infant brain. *Proceedings of the National Academy of Sciences of the United States of America*, *104*(39), 15531–15536.

Gao, W., Alcauter, S., Elton, A., Henandez-Castillo, C. R., Smith, J. K., Ramirez, J., & Lin, W. (2015). Functional network development during the first year: Relative Sequence and socioeconomic correlations. *Cerebral Cortex*, *25*(9), 2919–2928.

Gao, W., Alcauter, S., Smith, J. K., Gilmore, J., & Lin, W. (2015). Development of human brain cortical network architecture during infancy. *Brain Structure and Function*, *220*(2), 1173–1186.

Gao, W., Elton, A., Zhu, H., Alcauter, S., Smith, J. K., Gilmore, J. H., & Lin, W. (2014). Intersubject variability of and genetic effects on the brain's functional connectivity during infancy. *Journal of Neuroscience*, *34*, 11288–11296. https://doi.org/10.1523/JNEUROSCI.5072-13.2014

Gao, W., Gilmore, J. H., Giovanello, K. S., Smith, J. K., Shen, D., Zhu, H., & Lin, W. (2011). Temporal and spatial evolution of brain network topology during the first two years of life. *PLoS ONE*, *6*(9), e25278. https://doi.org/10.1371/journal.pone.0025278

Gao, W., Gilmore, J. K., Shen, D., Smith, J. K., Zhu, H., & Lin, W. (2013). The synchronization within and interaction between the default and dorsal attention networks in early infancy. *Cerebral Cortex*, *23*(3), 594–603.

Gao, W., Zhu, H., Giovanello, K. S., Smith, J. K., Shen, D., Gilmore, J. H., & Lin, W. (2009). Evidence on the emergence of the brain's default network from 2-week-old to 2-year-old healthy pediatric subjects. *Proceedings of the National Academy of Sciences of the United States of America*, *106*(16), 6790–6795.

Gillebert, C. R., & Mantini, D. (2013). Functional connectivity in the normal and injured brain. *Neuroscientist*, *19*, 509–522. https://doi.org/10.1177/1073858412463168

Goksan, S., Hartley, C., Hurley, S. A., Winkler, A. M., Eugene, P. D., Jenkinson, M., … Slater, R. (2017). Optimal echo time for functional MRI of the infant brain identified in response to noxious stimulation. *Magnetic Resonance in Medicine*, *78*(2), 625–631.

Graham, A. M., Pfeifer, J. H., Fisher, P. A., Lin, W., Gao, W., & Fair, D. A. (2015). The potential of infant fMRI research and the study of early life stress as a promising exemplar. *Developmental Cognitive Neuroscience*, *12*, 12–39.

Gratton, C., Laumann, T. O., Nielsen, A. N., Greene, D. J., Gordon, E. M., Gilmore, A. W., … Petersen, S. E. (2018). Functional brain networks are dominated by stable group and individual factors, not cognitive or daily variation. *Neuron*, *98*(2), 439–452.

Griffanti, L., Douad, G., Bijsterbosch, J., Evangelisti, S., Alfaro-Almagro, F., Glasser, M. F., … Smith, S. M. (2017). Hand classification of fMRI ICA noise components. *NeuroImage*, *154*, 188–205. https://doi.org/10.1016/j.neuroimage.2016.12.036

Griffanti, L., Salimi-Khorshidi, G., Beckmann, C. F., Auerbach, E. J., Douaud, G., Sexton, C. E., … Smith, S. M. (2014). ICA-based artefact removal and accelerated fMRI acquisition for improved resting state network imaging. *NeuroImage*, *95*, 232–247. https://doi.org/10.1016/j.neuroimage.2014.03.034

Horovitz, S. G., Braun, A. R., Carr, W. S., Picchioni, D., Balkin, T. J., Fukunaga, M., & Duyn, J. H. (2009). Decoupling of the brain's default mode network during deep sleep. *Proceedings of the National Academy of Sciences of the United States of America*, *106*(27), 11376–11381.

Huckins, J. F., Adeyemo, B., Miezin, F. M., Power, J. D., Gordon, E. M., Laumann, T. O., … Kelley, W. M. (2019). Reward-related regions form a preferentially coupled system at rest. *Human Brain Mapping*, *40*(2), 361–376.

Huotari, N., Raitamaa, L., Helakari, H., Kananen, J., Raatikainen, V., Rasila, A., … Korhonen, V. O. (2019). Sampling rate effects on resting state fMRI metrics. *Frontiers in Neuroscience*, *13*, 279. https://doi.org/10.3389/fnins.2019.00279

Hyvärinen, A. (1999). Fast and robust fixed-point algorithms for independent component analysis. *IEEE Transactions on Neural Networks*, *10*(3), 626–634.

Jenkinson, M., Bannister, P., Brady, J. M., & Smith, S. M. (2002). Improved optimisation for the robust and accurate linear registration and motion correction of brain images. *NeuroImage*, *17*(2), 825–841.

Jenkinson, M., & Smith, S. M. (2001). A global optimisation method for robust affine registration of brain images. *Medical Image Analysis*, *5*(2), 143–156. https://doi.org/10.1016/S1361-8415(01)00036-6

Kalcher, K., Boubela, R. N., Huf, W., Bartova, L., Kronnerwetter, C., Derntl, B., … Moser, E. (2014). The spectral diversity of resting-state fluctuations in the human brain. *PLoS ONE*, *9*(4), e93375. https://doi.org/10.1371/journal.pone.0093375

Karlsson, L., Tolvanen, M., Scheinin, N. M., Uusitupa, H. M., Korja, R., Ekholm, E., … Karlsson, H. (2018). Cohort profile: The FinnBrain Birth Cohort Study (FinnBrain). *International Journal of Epidemiology*, *47*(1), 15–16j. https://doi.org/10.1093/ije/dyx173

Khazaee, A., Ebrahimzadeh, A., & Babajani-Feremi, A. (2015). Identifying patients with Alzheimer's disease using resting-state fMRI and graph theory. *Clinical Neurophysiology*, *126*(11), 2132–2141.

Kim, J., Vaj Dijk, K. R., Libby, A., & Napadow, V. (2014). Frequency-dependent relationships between resting-state functional magnetic resonance imaging signal power and head motion is localized within distributed association networks. *Brain Connectivity*, *4*(1), 30–39.

Knickmeyer, R. C., Gouttard, S., Kang, C., Evans, D., Wilber, K., Smith, J. K., … Gilmore, J. H. (2008). A structural MRI study of human brain development from birth to 2 years. *Journal of Neuroscience*, *28*, 12176–12182. https://doi.org/10.1523/JNEUROSCI.3479-08.2008

Kwon, S. H., Scheinost, D., Lacadie, C., Sze, G., Schneider, K. C., Dai, F., … Ment, L. R. (2015). Adaptive mechanisms of developing brain: Cerebral lateralization in the prematurely-born. *NeuroImage*, *108*, 144–150.

Lara, A. H., & Wallis, J. D. (2015). The role of prefrontal cortex in working memory: A mini review. *Frontiers in Systems Neuroscience*, *9*, 173.

Larson-Prior, L. J., Zempel, J. M., Nolan, T. S., Prior, F. W., Snyder, A. Z., & Raichle, M. E. (2009). Cortical network functional connectivity in the descent to sleep. *Proceedings of the National Academy of Sciences of the United States of America*, *106*(11), 4489–4494.

Lee, W., Morgan, B. R., Shroff, M. M., Sled, J. G., & Taylor, M. J. (2013). The development of regional functional connectivity in preterm infants into early childhood. *Neuroradiology*, *55*(2), 105–111.

Lin, W., Zhu, Q., Gao, W., Chen, Y., Toh, C.-H., Styner, M., … Gilmore, J. H. (2008). Functional connectivity MR imaging reveals cortical functional connectivity in the developing brain. *American Journal of Neuroradiology*, *29*, 1883–1889. https://doi.org/10.3174/ajnr.A1256

Lowe, M. J., Mock, B. J., & Sorenson, J. A. (1998). Functional connectivity in single and multislice echoplanar imaging using resting-state fluctuations. *NeuroImage*, *7*(2), 119–132.

Marek, S., & Dosenbach, N. U. F. (2018). The frontoparietal network: Function, electrophysiology, and importance of individual precision mapping. *Dialogues in Clinical Neuroscience*, *20*(2), 133–144.

Mary, A., Wens, V., Op de Beeck, M., Leproult, R., De Tiege, X., & Peigneux, P. (2017). Resting-state functional connectivity is an age-dependent predictor of motor learning abilities. *Cerebral Cortex*, *27*(10), 4923–4932.

Mitra, A., Snyder, A. Z., Tagliazucchi, E., Laufs, H., Elison, J., Emergson, R. W., … Raichle, M., Jr. (2017). Resting-state fMRI in sleeping infants more closely resembles adult sleep than adult wakefulness. *PLoS ONE*, *12*(11), e0188122.

Mueller, S., Wang, D., Fox, M. D., Yeo, B. T., Sepulcre, J., Sabuncu, M. R., … Liu, H. (2013). Individual variability in functional connectivity architecture of the human brain. *Neuron*, *77*, 586–595. https://doi.org/10.1016/j.neuron.2012.12.028

Niazy, R. K., Xie, J., Miller, K., Beckmann, C. F., & Smith, S. M. (2011). Spectral characteristics of resting state networks. *Progress in Brain Research*, *193*, 259–276.

Pamilo, S., Malinen, S., Hlushchuk, Y., Seppä, M., Tikka, P., & Hari, R. (2012). Functional subdivision of group-ICA results of fMRI data collected during cinema viewing. *PLoS ONE*, *7*(7), e42000. https://doi.org/10.1371/journal.pone.0042000

Pan, W., Liu, C., Yang, Q., Gu, Y., Yin, S., & Chen, A. (2016). The neural basis of trait self-esteem revealed by the amplitude of low-frequency fluctuations and resting state functional connectivity. *Social Cognitive and Affective Neuroscience*, *11*(3), 367–376.

Power, J. D., Barnes, K. A., Snyder, A. Z., Schlaggar, B. L., & Petersen, S. E. (2012). Spurious but systematic correlations in functional connectivity MRI networks arise from subject motion. *NeuroImage*, *59*(3), 2142–2154.

Pruim, R. H. R., Mennes, M., van Rooij, D., Llera, A., Buitelaar, J. K., & Beckmann, C. F. (2015). ICA-AROMA: A robust ICA-based strategy for removing motion artifacts from fMRI data. *NeuroImage*, *112*, 267–277.

Pulli, E. P., Kumpulainen, V., Kasurinen, J. H., Korja, R., Merisaari, H., Karlsson, L., … Tuulari, J. J. (2018). Prenatal exposures of and infant brain: Review of magnetic resonance imaging studies and a population description analysis. *Human Brain Mapping*, *40*(6), 1987–2000. https://doi.org/10.1002/hbm.24480

Raichle, M. E. (2015). The brain's default mode network. *Annual Review of Neuroscience*, *38*(1), 433–447.

Ray, K. L., McKay, D. R., Fox, P. M., Riedel, M. C., Uecker, A. M., Beckmann, C. F., … Laird, A. R. (2013). ICA model order selection of task co-activation networks. *Frontiers in Neuroscience*, *10*(7), 237.

Reineberg, A. E., Andrews-Hanna, J. R., Depue, B. E., Friedman, N. P., & Banich, M. T. (2015). Resting-state networks predict individual differences in common and specific aspects of executive function. *NeuroImage*, *1*, 69–78.

Rosazza, C., & Minati, L. (2011). Resting-state brain networks: literature review and clinical applications. *Neurological Sciences*, *32*(5), 773–785.

Salimi-Khorshidi, G., Douaud, G., Beckmann, C. F., Glasser, M. F., Griffanti, L., & Smith, S. M. (2014). Automatic denoising of functional MRI data: Combining independent component analysis and hierarchical fusion of classifiers. *NeuroImage*, *90*, 449–468. https://doi.org/10.1016/j.neuroimage.2013.11.046

Shi, F., Yap, P. T., Wu, G., Jia, H., Gilmore, J. H., Lin, W., & Shen, D. (2011). Infant brain atlases from neonates to 1- and 2-year-olds. *PLoS ONE*, *6*(4), e18746. https://doi.org/10.1371/journal.pone.0018746

Smith, S. (2002). Fast robust automated brain extraction. *Human Brain Mapping*, *17*(3), 143–155. https://doi.org/10.1002/hbm.10062

Smith, S. M., Nichols, T. E., Vidaurre, D., Winkler, A. M., Behrens, T. E. J., Glasser, M. F., … Miller, K. L. (2015). A positive-negative mode of population covariation links brain connectivity, demographics and behavior. *Nature Neuroscience*, *18*, 1565–1567. https://doi.org/10.1038/nn.4125

Smitha, K. A., Akhil Raja, K., Arun, K. M., Rajesh, P. G., Thomas, B., Kapilamoorthy, T. R., & Kesavadas, C. (2017). Resting state fMRI: A review on methods in resting state connectivity analysis and resting state networks. *The Neuroradiology Journal*, *30*(4), 305–317.

Smith-Collins, A. P. R., Luyt, K., Heep, A., & Kauppinen, R. A. (2015). High frequency functional brain networks in neonates revealed by rapid acquisition resting state fMRI. *Human Brain Mapping*, *36*(7), 2483–2494.

Smyser, C. D., Inder, T. E., Shimony, J. S., Hill, J. E., Degnan, A. J., Snyder, A. Z., & Neil, J. J. (2010). Longitudinal analysis of neural network development in preterm infants. . *Cerebral Cortex*, *20*(12), 2852–2862.

Smyser, C. D., & Neil, J. J. (2015). Use of resting state functional MRI to study brain development and injury in neonates. *Seminars in Perinatology*, *39*(2), 130–140.

Tagliazucchi, E., von Wegner, F., Morzelewski, A., Brodbeck, V., Jahnke, K., & Laufs, H. (2013). Breakdown of long-range temporal dependence in default mode and attention networks during deep sleep. *Proceedings of the National Academy of Sciences of the United States of America*, *110*(38), 15419–15424.

Takeuchi, H., Taki, Y., Nouchi, R., Hashizume, H., Sekiguchi, A., Kotozaki, Y., … Kawashima, R. (2013). Effects of working memory training on functional connectivity and cerebral blood flow during rest. *Cortex*, *49*, 2106–2125. https://doi.org/10.1016/j.cortex.2012.09.007

Takeuchi, H., Taki, Y., Nouchi, R., Hashizume, H., Sekiguchi, A., Kotozaki, Y., … Kawashima, R. (2014). Effects of multitasking-training on gray matter structure and resting state neural mechanisms. *Human Brain Mapping*, *35*(8), 3646–3660.

Tambini, A., Ketz, N., & Davachi, L. (2010). Enhanced brain correlations during rest are related to memory for recent experiences. *Neuron*, *65*, 280–290. https://doi.org/10.1016/j.neuron.2010.01.001

Telkemeyer, S., Rossi, S., Koch, S. P., Nierhaus, T., Steinbrink, J., Poeppel, D., … Wartenburger, I. (2009). Sensitivity of newborn auditory cortex to the temporal structure of sounds. *Journal of Neuroscience*, *29*(47), 14726–14733.

Thomas, J. L., Spassky, N., Perez Villegas, E. M., Olivier, C., Cobos, I., Couje-Zalc, C., … Zalc, B. (2000). Spatiotemporal development of oligodendrocytes in the embryonic brain. *Journal of Neuroscience Research*, *59*(4), 471–476. https://doi.org/10.1002/(SICI)1097-4547(20000215)59:4<471:AID-JNR1>3.0.CO;2-3

Volpe, J. J. (2008). Neuronal proliferation, migration, organization and myelination. In T. E. Inder, B. T. Darras, L. S. de Vries, A. J. du Plessis, J. J. Neil, & J. M. Perlman (Eds.), *Neurology of the newborn* (6th ed., pp. 51–118). Philadelphia, PA: Saunders Elsevier Inc.

Wang, Y., Ramsey, R., & Hamilton, A. F. (2011). The control of mimicry by eye contact is mediated by medial prefrontal cortex. *Journal of Neuroscience*, *31*(33), 12001–12010.

Wylie, K. P., Rojas, D. C., Ross, R. G., Hunter, S. K., Maharajh, K., Cornier, M.-A., & Tregellas, J. R. (2014). Reduced brain resting-state network specificity in infants compared with adults. *Neuropsychiatric Disease and Treatment*, *10*, 1349–1359.

Xu, Y., Cao, M., Laio, X., Xia, M., Wang, X., Jeon, T., … He, Y. (2019). Development and emergence of individual variability in the functional connectivity architecture of the preterm human brain. *Cerebral Cortex*, *29*(10), 4208–4222. https://doi.org/10.1093/cercor/bhy302

Zhang, H., Shen, D., & Lin, W. (2019). Resting-state functional MRI studies on infant brains: A decade of gap-filling efforts. *NeuroImage*, *185*, 664–684.

Zhao, Z., Huang, T., Tang, C., Ni, K., Pan, X., Yan, C., … Luo, Y. (2017). Altered resting-state intra- and inter- network functional connectivity in patients with persistent somatoform pain disorder. *PLoS ONE*, *12*(4), e0176494. https://doi.org/10.1371/journal.pone.0176494

SUPPORTING INFORMATION

Additional Supporting Information may be found online in the Supporting Information section.

How to cite this article: Rajasilta O, Tuulari JJ, Björnsdotter M, et al. Resting-state networks of the neonate brain identified using independent component analysis. *Develop Neurobiol*. 2020;00:1–15. https://doi.org/10.1002/dneu.22742